World Academy of Science, Engineering and Technology
International Journal of Chemical and Molecular Engineering
Vol:11, No:2, 2017

Comparative Studies of the Effects of Microstructures on the Corrosion Behavior of Micro-Alloyed Steels in Unbuffered 3.5 Wt% NaCl Saturated with CO_2

Lawrence I. Onyeji, Girish M. Kale, M. Bijan Kermani

***Abstract*—**Corrosion problem which exists in every stage of oil and gas production has been a great challenge to the operators in the industry. The conventional carbon steel with all its inherent advantages has been adjudged susceptible to the aggressive corrosion environment of oilfield. This has aroused increased interest in the use of micro alloyed steels for oil and gas production and transportation. The corrosion behavior of three commercially supplied micro alloyed steels designated as A, B, and C have been investigated with API 5L X65 as reference samples. Electrochemical corrosion tests were conducted in an unbuffered 3.5 wt% NaCl solution saturated with CO_2 at 30 ^{0}C for 24 hours. Pre-corrosion analyses revealed that samples A, B and X65 consist of ferrite-pearlite microstructures but with different grain sizes, shapes and distribution whereas sample C has bainitic microstructure with dispersed acicular ferrites. The results of the electrochemical corrosion tests showed that within the experimental conditions, the corrosion rate of the samples can be ranked as $CR_{(A)} < CR_{(X65)} < CR_{(B)} < CR_{(C)}$. These results are attributed to difference in microstructures of the samples as depicted by ASTM grain size number in accordance with ASTM E112-12 Standard and ferrite-pearlite volume fractions determined by ImageJ Fiji grain size analysis software.

***Keywords*—**Carbon dioxide corrosion, corrosion behavior, micro-alloyed steel, microstructures.

I. Introduction

CARBON steel because of its well-known advantages such as low cost, availability, good mechanical properties etc. [1], [2], are mostly used as structural materials for oil and gas facilities. Another attraction of carbon steel in this industry is that the surface is covered by protective corrosion product films [1], [3]. Edmonds and Cochrane [4] therefore declared that about 95% of the construction materials used in oil and gas industries is carbon steel. However, all these inherent advantages do not protect carbon steel in harsh and hostile (acidic or alkaline) environments of oil and gas industries [1], [5]. These disadvantages of carbon steel are caused by its high corrosivity which affects the capital expenditure (CAPEX), operational expenditure (OPEX) and health and safety environment (HSE) of oil and gas industry [6]. Effort to then replace carbon steel through the use of corrosion resistant alloys (CRAs) such as 13% Cr-steels, the various types of duplex stainless steels and/or higher alloyed steels is about 3-15 times more expensive when compared to carbon steels [3]-[5], [7], [8]. Therefore, there has been an increased research to alter the internal structures and/or surface morphology of carbon steels in order to develop materials with appropriate properties that can withstand the corrosive environment in oilfield and at low cost. This has necessitated the development of micro alloyed steels. Micro alloyed steels are designed to provide special desirable combination of mechanical properties such as strength, toughness, formability, weldability and greater atmospheric corrosion resistance than conventional carbon steel [9]. This excellent combination of properties are made possible by the presence of fine grain size occasioned by adding micro quantity of alloying elements, controlled rolling and application of appropriate processing technologies and heat treatments [9].

Corrosion problems exist in every stage of oil and gas production [6] and they manifest themselves in several forms which include carbon dioxide (sweet) corrosion, hydrogen sulphide (sour) corrosion in the produced fluids and corrosion by oxygen in water injection [6], [8], [10], [11] with their attendant enormous cost [10]. It then follows that the understanding, prediction and control of corrosion are the key challenges of the operators in the oil and gas industry. Among these forms of corrosion, CO_2 is the most prevalent accounting for about 60% of oilfield failures [3], [6], [8], [10], [11]. Although there are still some grey areas among researchers with regards to rate determining steps [3], [12], the mechanism of CO_2 corrosion in oil and gas industry has been studied in depth and different proposals developed and published [3], [8], [12]-[19] These variety of models are attributed to the complexities of the processes involved in CO_2 corrosion [17], [20]. Confirming this complexities, Dugstad [3] stated that CO_2 corrosion does not depend on one mechanism but on some chemical, electrochemical and physical processes that occur simultaneously. Thus, for adequate explanation and understanding of CO_2 corrosion mechanism, all these processes must be taken into consideration. Although there are diverse proposals, all generally agreed on the dissolution of iron at the anode and the evolution of hydrogen gas through

L. I. Onyeji is a Postgraduate Student with the School of Chemical and Process Engineering, University of Leeds, LS2 9JT, UK. (corresponding author; phone: 07466099454; e-mail: pmlio@leeds.ac.uk).

G. M. Kale is Fellow of Institutes of Materials, Minerals and Mining (UK), is an Associate Professor and Reader in Solid State Ionics with the Institutes for Materials Research, School of Chemical and Process Engineering, University of Leeds, LS2 9JT, UK.

B. M. Kermani is a Visiting Professor at the School of Chemical and Process Engineering, University of Leeds, LS2 9JT, UK.

any of the three cathodic reactions involving the reduction of either H^+, H_2CO_3 or H_2O depending on the acidity of the solution [3], [8], [12], [14]. The first and most widely used CO_2 corrosion mechanism was proposed by de Waard et al. [13] which can be expressed as:

$$H_2CO_3 + e^- \rightarrow H + HCO_3^- \quad (1)$$

$$2H \rightarrow H_2 \quad (2)$$

With the iron oxidizing at the anode as

$$Fe \rightarrow Fe^+ + e^- \quad (3)$$

The overall reaction then is expressed as

$$Fe + CO_2 + H_2O \rightarrow FeCO_3 + H_2 \quad (4)$$

API 5L X65 was used as reference sample in this work because some authors [7], [8], [21] adjudged it as one of the most widely accepted and used material for production and transportation of oil and gas. This paper, which is the first in the series of work aimed at subjecting commercially supplied proprietary steel grades to thermo-mechanical and chemical treatments to improve their corrosion resistance beyond that of X65, shall use potentiodynamic polarization techniques (LPR and Tafel Plot) to compare the corrosion propensity of the proprietary steels with that of X65.

II. Experimental

A. Materials

The chemical compositions of the three commercially supplied proprietary steel grades and that of the reference sample (X65) are shown in Table I. Depending on the As-supplied profile, the steel grades were cut into sizable dimensions. Samples A and X65 were cut into 25 mm diameter and 5 mm thickness while samples B and C were cut to 18 mm x 16 mm x 5 mm and 18 mm x 16 mm x 8 mm, respectively.

TABLE I
Elemental Specifications of the Samples

Sample	C	Mn	S	P	Si	Cr	Fe
A	0.12	1.27	0.002	0.008	0.18	0.11	Balance
B	0.22	1.4	0.001	0.012	0.32	0.25	Balance
C	0.25	0.54	0.001	0.01	0.26	0.99	Balance
X65	0.12	1.27	0.002	0.008	0.18	0.11	Balance

B. Sample Preparations

The cut specimens were soldered at the back with insulated copper wires before enclosing with non-conduction resin. This resin helped in handling the specimen during grinding and polishing. The resin also covered all surfaces of the specimen leaving only one surface that act as the working electrodes. Grinding was achieved using silicon carbide (SiC) grit paper. Five sizes P120, P320, P600, P800 and P1200 of SiC grit papers were used respectively. This gave an increasing successive abrasive fineness. The specimens after grinding were degreased with acetone, rinsed with distilled water, dried with compressed air and immediately immersed into the electrolyte for electrochemical tests.

The ground specimens for OM and SEM/EDX analyses were further polished using 5 µm, 3 µm and 1 µm abrasive diamond slurry, degreased with acetone, rinsed with distilled water and dried with compressed air. The final polished surfaces were etched with 2% nital and analyzed using OM and SEM/EDX. The grain size of each sample was measured using ImageJ Fiji grain size analysis software and the grain size number calculated using the planimeteric procedures as outlined in ASTM E112–12 standard [22]

C. Electrochemical Corrosion Tests

All the electrochemical corrosion tests were performed in unbuffered 3.5 wt% NaCl solution saturated with carbon dioxide (CO_2) at 30 °C and for 24 hours. Linear polarization resistance (LPR) measurements were conducted within the scan range of ±15 mV verses open circuit potential (OCP) and a scan rate of 0.25 mV/Sec. Each of the four samples were polarized in triplicate in order to ensure reproducibility. The anodic and cathodic branches of Tafel plots were conducted separately at the end of the 24 hours LPR with a sweep range of ±250 mV verses OCP and a scan rate of 0.5 mV/Sec. At the end of each experiments, the samples were carefully removed from the cell, washed with de-ionized water, dried with compressed air and taken for surface analyses and characterization using SEM/EDX.

III. Results and Discussions

A. Metallographic Studies of the Micro alloyed Samples

Optical Microscope (OM) and Scanning electron Microscopy/Energy Dispersion X-ray Spectroscopy (SEM/ EDX) were used to characterize both the pre-corroded and post corroded samples. Fig. 1 shows the optical microscope whereas Fig. 2 shows the SEM micrograph of the as-received samples. All the OM and SEM micrographs have the same magnification with higher magnification overlaid for clarity.

It is interesting to note that all the samples have different microstructures. Some authors [23]-[25] attributed this to the chemical composition and the thermo-mechanical treatment applied on the individual samples during manufacturing processes. However, a closer observation of Figs. 1 and 2 revealed that samples X65, A and B have light and dark zones which are believed to be colonies of pearlite in ferrite matrix [23]. These ferrite and pearlite phases consist of grains whose sizes, shapes and distributions are relatively uniform within each sample but differ among samples. The micrographs have the same magnifications. The grain size number of the samples calculated according to ASTM E112-12 Standard are shown in Table II. This table also shows that the grain sizes of the three samples can be ranked as B < X65 < A. This ranking format also sufficed for ferrite -pearlite volume ratio. Sample B has higher carbon content and so in line with the reports of Zhao et al. [26] and Ochoa [24], increase in carbon content

favors the formation of pearlite (ferrite-cementite mixture). Although samples X65 and A has almost similar chemical composition, the difference in microstructures can majorly be attributed to the thermo-mechanical treatment applied during their manufacturing as reasoned above [23]-[25].

TABLE II
ASTM GRAIN SIZE NUMBER AND FERRITE/PEARLITE RATIO (%) FOR THE SAMPLES

Samples	A	X65	B	C
ASTM Grain Size No.	3.89	4.5	5.57	5.77
Ferrite/Pearlite (%)	63.61	57.48	48.2	
Average Grain Size (um)	68.54	46.63	20.6	14.67

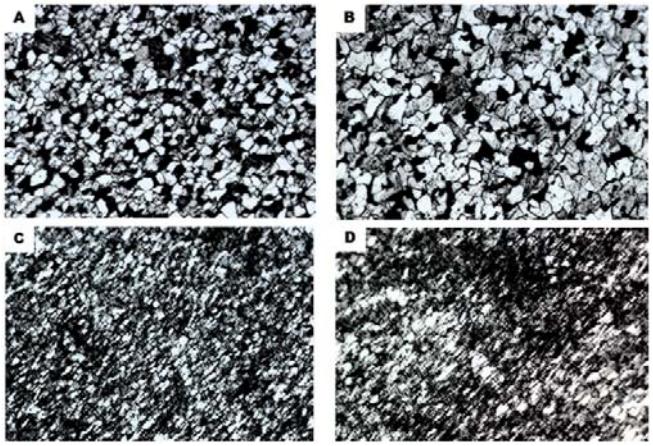

Fig. 1 Optical Micrographs of As-Received Samples at 20 magnification (A) X65, (B) Sample A, (C) Sample B and (D) Sample C

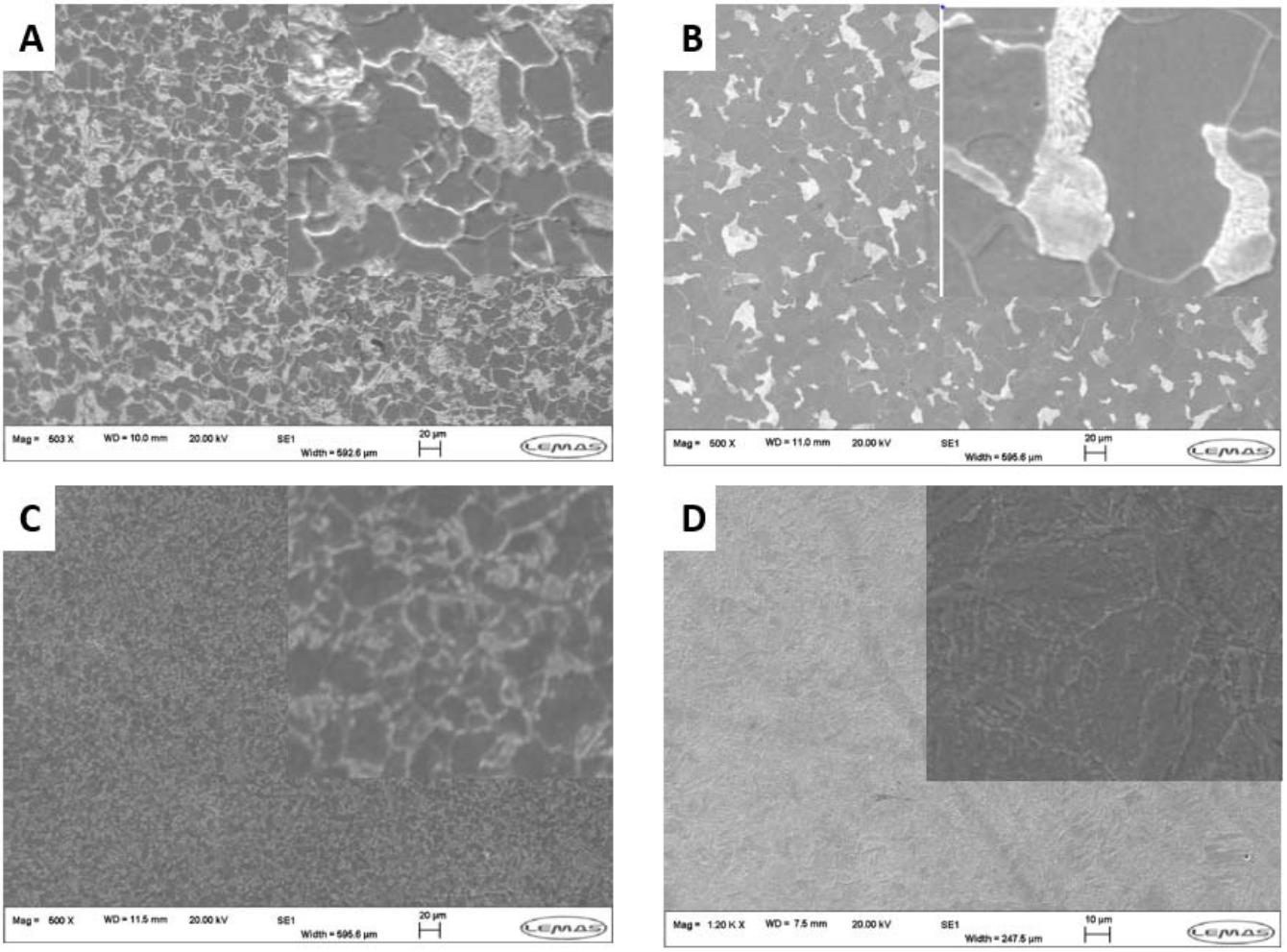

Fig. 2 SEM Micrographs of As-Received Samples at 500 (2000 magnification overlaid) (A) X65, (B) Sample A, (C) Sample B and (D) Sample C

The optical and SEM micrographs of Sample C shown in Figs. 1 (D) and 2(D) respectively revealed bainitic structure with some evenly distributed acicular ferrites [27]. Many authors [25], [27]-[29], reported that bainitic structures are formed when the decomposition of austenite to ferrite- pearlite structure is restrained by the presence of micro alloying elements. Agreeing with this, Kermani and Morshed [7] and Kermani et al. [8] specifically affirmed that Cr and Mo delay

and retard decomposition of martensite and austenite into ferrites and carbides upon tempering. This is attributed to the sluggish diffusion process of the micro-additions to forming carbides. Sample C contains more Cr (0.99 wt%) and Mo (0.46 wt%) than the other samples. This must have necessitated the formation of bainitic structure.

B. LPR Measurement

ACM Gill 12 potentiostat was used to conduct linear polarization measurement of the samples. Each of the samples (working electrode) were polarized within the range of ±15 mV versus OCP at a scan rate of 0.25 mV/Sec for 24 hour in an unbuffered 3.5 wt% NaCl solution saturated with CO_2 at 30 °C. Each of the samples was polarized at least three times to ensure reproducibility and the average corrosion rate values were plotted against time as shown in Fig. 3. Also Fig. 4 shows the plots of variation of corrosion potential with time. This figure shows that within the experimental conditions, the average general corrosion rate for each of the samples increased almost linearly with time throughout the 24 hours tests. This is a strong suggestion of metal dissolution as observed by Nesic [15] and reveals that the corrosion resistance of the samples can be ranked as Sample C < Sample B < X65 < Sample A. This trend was also corroborated by the plots of the average corrosion potential with time as shown in Fig. 4. These variations in corrosion rate and corrosion potentials of the samples can be attributed to their chemical composition, the thermo-mechanical treatment applied during manufacturing and the attendant microstructures formed. This is in agreements with the results of many researchers [3], [11], [23]-[25], [30]. The effects of microstructures in determining the corrosion rate is more pronounced at temperatures below 60 °C when protective corrosion products ($FeCO_3$) are not formed or if formed they are porous and un-protective therefore corrosion rate increases with temperature [25].

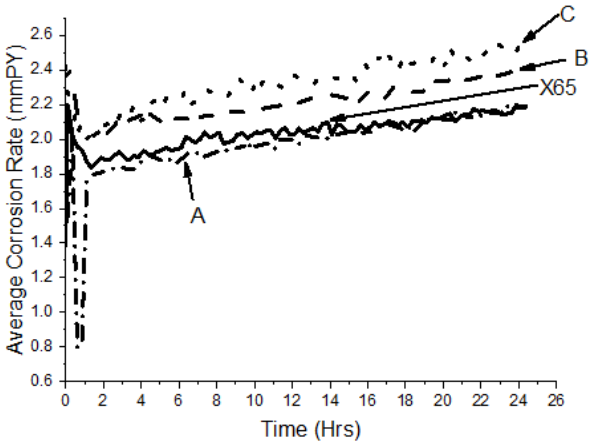

Fig. 3 Average Corrosion Rate of Samples in unbuffered 3.5 wt% NaCl Saturated with CO_2, 30 °C, 250 rpm for 24 Hrs

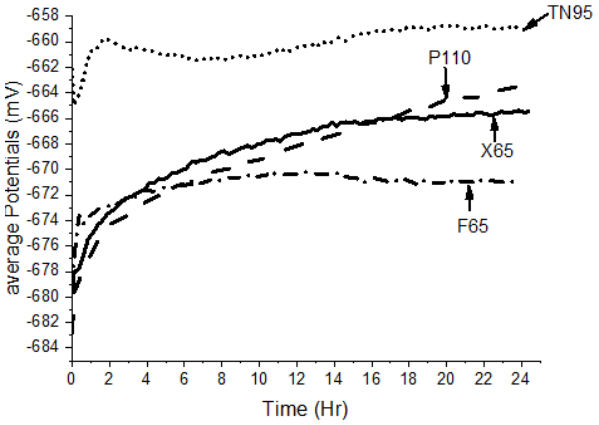

Fig. 4 Average Potential of Samples in unbuffered 3.5 wt% NaCl Saturated with CO_2, 30 °C, 250 rpm for 24 Hrs

In the ferrite-Pearlite (**α**-Fe + Fe_3C) microstructures such as in samples X65, A and B, Fe_3C is more cathodic than ferrite and has lower over-potential for hydrogen evolution. This leads to the formation of micro-galvanic cells with the selective dissolution of ferrite leaving Fe_3C exposed to the electrolyte as large cathodic sites which in turn increases corrosion rate [11], [15], [25], [31]. Thus more Fe_3C content signifies more cathodic sites which in turn lead to increase in corrosion rate. This must be why sample B with the highest grain size number and the least ferrite/pearlite volume ratio showed the least corrosion resistance than Samples X65 and A.

Samples X65 and A have almost similar chemical composition and so the difference in microstructure must have been majorly due to thermo-mechanical treatments applied in the manufacturing process. Table II shows that X65 has higher ASTM grain size number (smaller grains) and less ferrite/pearlite volume ratio than Sample A. This means that X65 has more cathodic sites and so exhibited less corrosion resistance than Sample A.

Fig. 5 shows the SEM images of the surfaces of the samples corroded in an unbuffered CO_2 saturated 3.5 wt% NaCl solution at 30 °C, 250 rpm and for 24 hours.

A keen observation of Figs. 5 (A) and (C) shows a network of non-oxidized laminar structures of Fe_3C exposed to the electrolyte where it acts as cathode enhancing further corrosion process. Dugstad et al. [32] reported that smaller carbide particles have the tendency to stick together and form networks. On the other hand, Fig. 5 (B) shows a situation where the non-oxidized Fe_3C particles were large and so did not form carbide network but remain discrete with lower surface area and so lower corrosion rate. This is in agreement with the view of Dugstad et al. [32].

Fig. 5 (D) shows the SEM micrographs of corroded Sample C. This micrographs reveals a sludge like corrosion product. This corrosion product according to Zhao [26] is very thin, non-adhesive and cracks easily thus rendering it un-protective against corrosion attack since it allows the ingress of electrolyte to continue corrosion. From the metallurgical point of view, sample C has high Cr and Mo content. These

elements according to some authors [7], [8], [25], [27] improve corrosion resistance by favoring passivity. However, this was not observed in TN95 because of high carbon content which formed carbides with undissolved Cr [4], [7], [32] leading to increased cathodic site and so increased corrosion rate [25], [27].

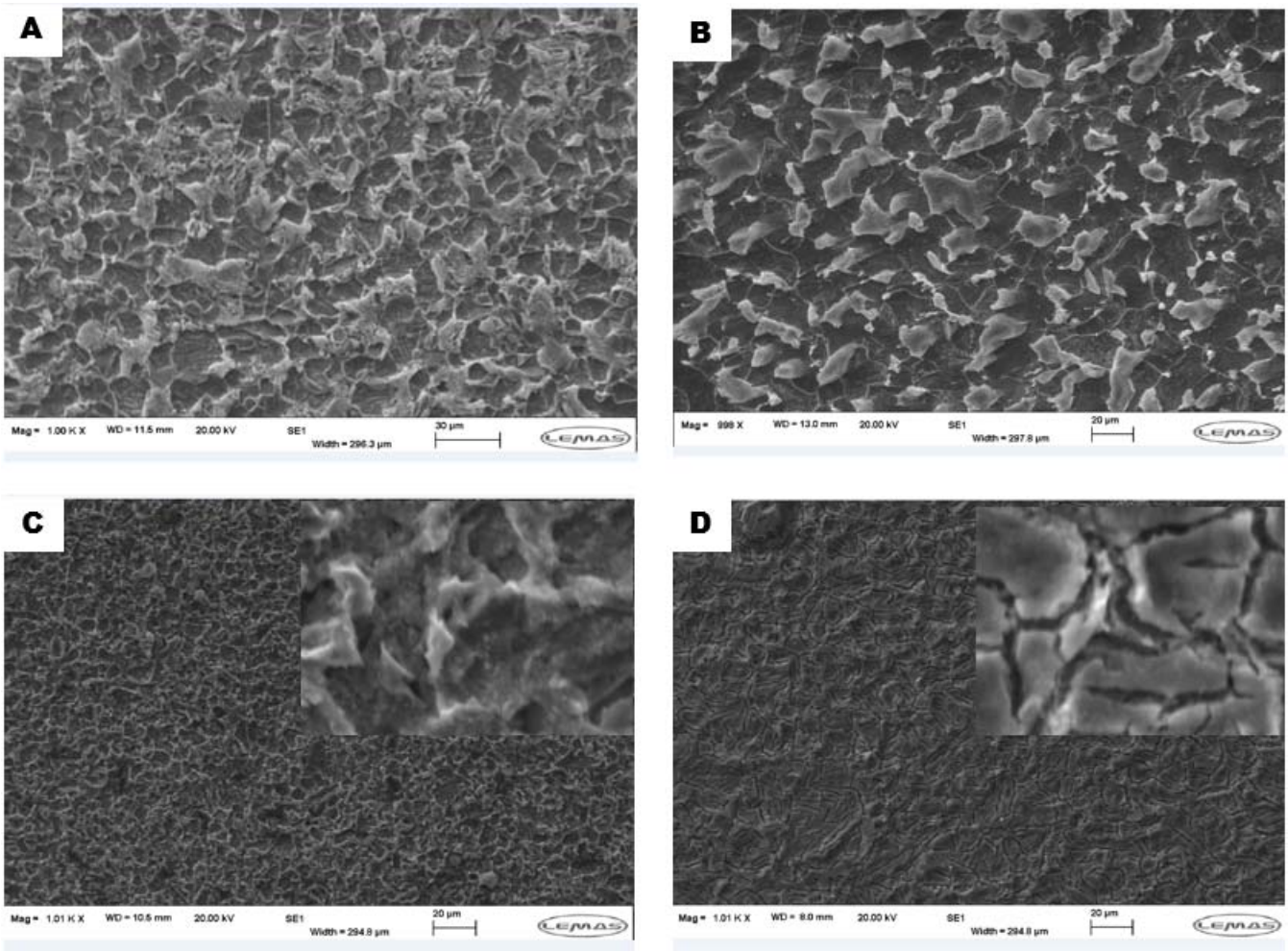

Fig. 5 SEM Micrograph of Corroded Samples in an unbuffered 3.5 wt% NaCl Saturated with CO_2, 30 ^{0}C and 250 rmp (A) X65, (B) Sample A, (C) Sample B and (D) Sample C

The EDX micro-analysis taken from the dark and light zones in the SEM micrographs for all samples reveal Fe, C and O as the main elements with Mn, Mo, V, Nb etc in traces. This is a strong suggestion of the presence of $FeCO_3$ but literature [3], [14], [15], [18], [24], [32] adjudged that protective corrosion products ($FeCO_3$) cannot form at temperatures below 60 °C. Also XRD spectra analyses reveal only Fe peaks with Fe_3C evenly dispersed at the base of the peak. It can then be concluded that traces of $FeCO_3$ which are very porous and so cannot effect any protection [18] may have begun to form but was not detected by the XRD analysis.

Based on the experimental conditions within the period under review, it can be concluded that all the experiments were scale-free CO_2 corrosion [33]. This is because the experiments were performed at pH < 4 and 30 °C. At these conditions, CO_2 corrosion product ($FeCO_3$) cannot form [3], [14], [15], [18], [24], [32] instead the basic anodic reaction is the dissolution (oxidation) of iron as in (5):

$$Fe \rightarrow Fe^{2+} + 2e^{-} \quad (5)$$

whereas the basic cathodic reaction is the evolution of hydrogen as in (6):

$$2H^{+} + 2e^{-} \rightarrow H_2 \quad (6)$$

C. Tafel Polarization Measurement

Tafel polarization measurements were conducted on each of the samples at the end of the 24 hours LPR. The anodic and cathodic branches of the Tafel plot were performed separately and the data plotted on a corrosion potential (E_{Corr}) versus log of corrosion current density (i_{Corr}). The Tafel constants (β_A and β_C) were estimated using the best line fit extrapolation techniques as outlined in ASTM G 102 - 89 [34], [35]. Fig. 6 shows the Tafel plots for the samples. The polarization parameters obtained from the curves are shown in Table III. The corrosion current density (i_{Corr}) of each sample was determined graphically by extrapolating cathodic and anodic

Tafel slopes to the (E_{Corr}) as shown in Fig. 7 with sample X65 as an example.

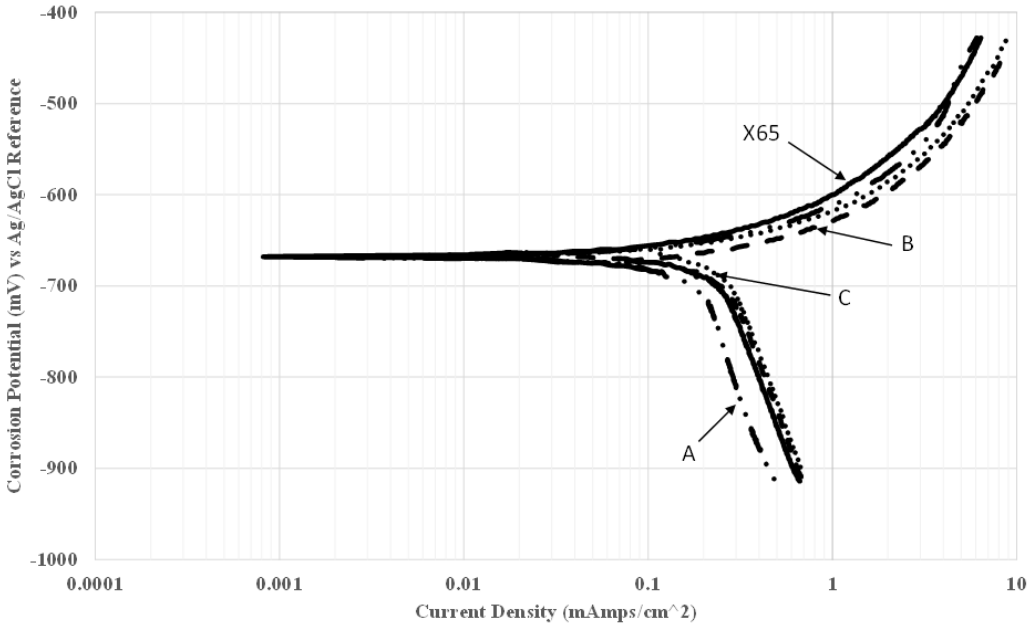

Fig. 6 Average Tafel Plots of the four Samples in unbuffered 3.5 wt% NaCl Saturated with CO_2, 30 °C, 250 rpm for 24 Hrs

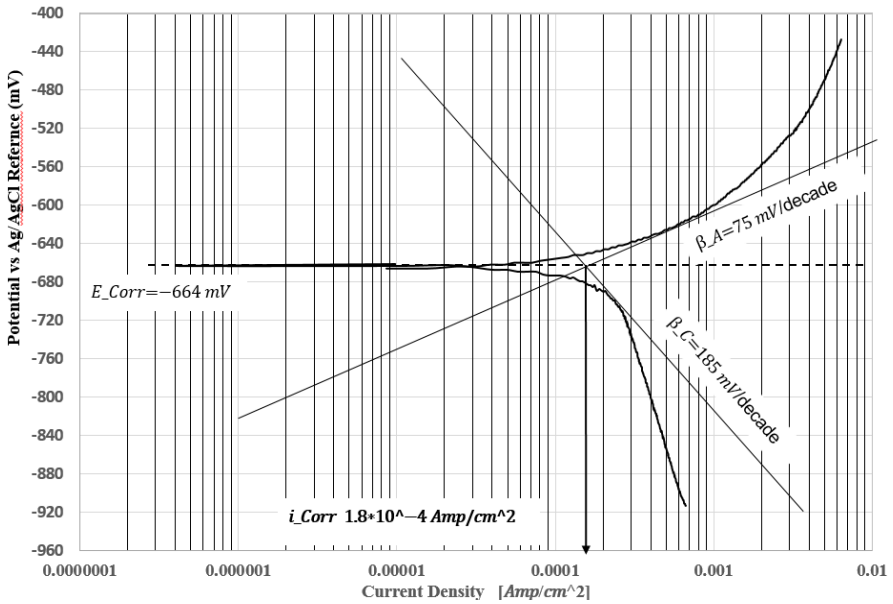

Fig. 7 Tafel Plots of X65 indicating how polarization parameters were determined

TABLE III
POTENTIODYNAMIC PARAMETERS OF THE SAMPLES ESTIMATED FROM TAFEL PLOTS

Sample	E_{Corr} (mV)	ICorr (mA/ cm^2)	β_A (mV/ dec)	B_C (mV/ dec)	Rp (Ω cm^2)	CR (mm/Y)
X65	-664	0.18	75	185	128.7	2,11
A	-672	0.17	65	240	130.6	1.99
B	-657	0.19	70	225	122.0	2.23
C	-675	0.2	65	275	114.1	2.35

Corrosion rates were also calculated using average values of LPR polarization resistance (Rp) and average LPR corrosion current density (i_{Corr}). The corrosion rates calculated from these three routes relatively have the same values as can be observed in Fig. 8. This therefore attests to the consistency in the trend of corrosion behavior of the samples within the experimental conditions.

The corrosion rates in Table III and schematically in Fig. 8 showed the same corrosion behavior trend exhibited by the samples in the LPR tests and the analyses based on the

microstructures of the samples. It can therefore be concluded that the corrosion rate of the samples can be ranked as $CR_{(A)} < CR_{(X65)} < CR_{(B)} < CR_{(C)}$.

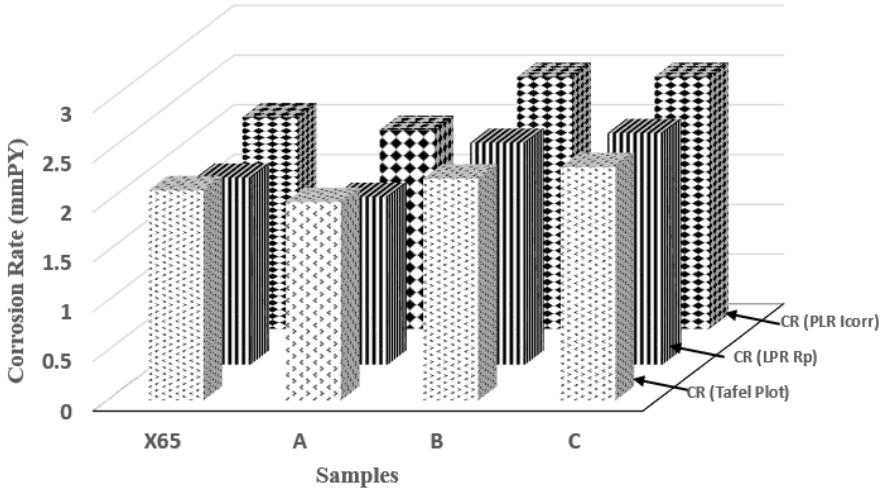

Fig. 8 Corrosion Rate Calculated from Estimated Tafel Parameters (CR Tafel Plot), Average Polarization Resistance (Rp) value from LPR and Average Current Density value from LPR

IV. Conclusions

The corrosion behaviour of three commercially supplied proprietary steel grades (Samples A, B, and C) and X65 as reference sample have been investigated in unbuffered 3.5 wt% NaCl solution saturated with CO_2 at 30 °C and for 24 hours. With these conditions, the LPR tests showed that there was a steady (almost linear) increase in general corrosion with time for all the four samples. This means a continuous metal dissolution with time which is typical of activation control reactions for systems at less than 60 °C and low pH (< 4). At these conditions, corrosion product film ($FeCO_3$) cannot form. Also the corrosion rate calculated using Tafel polarization technique reveals that Sample A = 1.99 mmPY, X65 = 2.11 mmPY, Sample B = 2.23 mmPY and Sample C = 2.35 mmPY giving the ranking of the samples as $CR_{(A)} < CR_{(X65)} < CR_{(B)} < CR_{(C)}$. The ASTM grain size number and the ferrite/pearlite volume ratio agreed with this ranking format. This can be attributed to difference in microstructures where micro-galvanic cells formed between ferrites which act as anode and cementite which act as cathode. This influenced the kinetic of corrosion process leading to selective dissolution of ferrite while leaving the non-dissolved cementite (Fe_3C) which increased cathodic sites. Thus the corrosion resistance of the samples decreased as the ferrite/pearlite volume ratio decreased.

References

[1] Ilman, M., *Analysis of internal corrosion in subsea oil pipeline.* Case Studies in Engineering Failure Analysis, 2014. 2(1): p. 1-8.

[2] Suárez Bermejo, J.C. and M.A. Herreros Sierra, *New fiber-metal hybrid laminated material, MALECON.* 2008.

[3] Dugstad, A. *Fundamental aspects of CO_2 metal loss corrosion-part 1: mechanism* in *CORROSION 2006*. 2006. NACE International.

[4] Edmonds, D.V. and R.C. Cochrane, *The effect of alloying on the resistance of carbon steel for oilfield applications to CO_2 corrosion.* Materials Research, 2005. 8(4): p. 377-385.

[5] Edelugo, S., *The timed response of different types of GRP laminates on exposure to various strengths of alkaline and acidic environments.* Journal of advanced materials, 2009. 41(2): p. 79-87.

[6] El-Lateef, H.A., et al., *Corrosion protection of steel pipelines against CO_2 corrosion—a review.* Chem. J, 2012. 2(2): p. 52-63.

[7] Kermani, B., et al. *Development of low carbon Cr-Mo steels with exceptional corrosion resistance for oilfield applications.* in *CORROSION 2001*. 2001. NACE International.

[8] Kermani, M. and A. Morshed, *Carbon dioxide corrosion in oil and gas production-A compendium.* Corrosion, 2003. 59(8): p. 659-683.

[9] Davis, J.R., *Alloying: understanding the basics.* 2001: ASM international.

[10] Popoola, L.T., et al., *Corrosion problems during oil and gas production and its mitigation.* International Journal of Industrial Chemistry, 2013. 4(1): p. 1-15.

[11] Lopez, D., T. Perez, and S. Simison, *The influence of microstructure and chemical composition of carbon and low alloy steels in CO_2 corrosion. A state-of-the-art appraisal.* Materials & Design, 2003. 24(8): p. 561-575.

[12] Schmitt, G. and M. Horstemeier. *Fundamental aspects of CO_2 metal loss corrosion-Part II: Influence of different parameters on CO_2 corrosion mechanisms* in *CORROSION 2006*. 2006. NACE International.

[13] De Waard, C. and D. Milliams, *Carbonic acid corrosion of steel.* Corrosion, 1975. 31(5): p. 177-181.

[14] Nesic, S., et al. *Electrochemical properties of iron dissolution in the presence of CO_2-basics revisited* in *CORROSION 96*. 1996. NACE International.

[15] Nešić, S., *Key issues related to modelling of internal corrosion of oil and gas pipelines–A review.* Corrosion Science, 2007. 49(12): p. 4308-4338.

[16] Fang, H., B. Brown, and S. Nešic, *Sodium chloride concentration effects on general CO_2 corrosion mechanisms.* Corrosion, 2013. 69(3): p. 297-302.

[17] Mishra, B., et al., *Development of a predictive model for activation-controlled corrosion of steel in solutions containing carbon dioxide.* Corrosion, 1997. 53(11): p. 852-859.

[18] Nesic, S., J. Postlethwaite, and S. Olsen, *An electrochemical model for prediction of corrosion of mild steel in aqueous carbon dioxide solutions.* Corrosion, 1996. 52(4): p. 280-294.

[19] Nordsveen, M., et al., *A mechanistic model for carbon dioxide corrosion of mild steel in the presence of protective iron carbonate films-Part 1: Theory and verification.* Corrosion, 2003. 59(5): p. 443-456.

[20] Ogundele, G. and W. White, *Some observations on corrosion of carbon steel in aqueous environments containing carbon dioxide.* Corrosion, 1986. 42(2): p. 71-78.

[21] David, E., C. Robert, and G. Rosa, *Effect of microalloying, principally with vanadium, processing conditions and microstructure on resistance*

to CO_2 corrosion. Journal of Iron and Steel Research (International), 2011. 1.
[22] E-112, A., *Standard test methods for determining average grain size*. 2010, ASTM International USA.
[23] Lopez, D.A., S. Simison, and S. De Sanchez, *The influence of steel microstructure on CO_2 corrosion. EIS studies on the inhibition efficiency of benzimidazole.* Electrochimica Acta, 2003. 48(7): p. 845-854.
[24] Ochoa, N., et al., *CO_2 corrosion resistance of carbon steel in relation with microstructure changes.* Materials Chemistry and Physics, 2015. 156: p. 198-205.
[25] Al-Hassan, S., et al., *Effect of microstructure on corrosion of steels in aqueous solutions containing carbon dioxide.* Corrosion, 1998. 54(6): p. 480-491.
[26] Zhao, Y., et al., *The mechanical properties and corrosion behaviors of ultra-low carbon microalloying steel.* Materials Science and Engineering: A, 2007. 454: p. 695-700.
[27] Vera, R., F. Vinciguerra, and M. Bagnara, *Comparative study of the behavior of API 5L-X65 grade steel and ASTM A53-B grade steel against corrosion in seawater.* Int. J. Electrochem. Sci, 2015. 10: p. 6187-6198.
[28] Morrison, W. *Overview of microalloying in steel*. in *The proceedings of the vanitec symposium, Guilin, China*. 2000.
[29] Matlock, D. and J. Speer, *Microalloying concepts and application in long products.* Materials Science and Technology, 2009. 25(9): p. 1118-1125.
[30] Palacios, C. and J. Shadley, *Characteristics of corrosion scales on steels in a CO_2-saturated NaCl brine.* Corrosion, 1991. 47(2): p. 122-127.
[31] Tanupabrungsun, T., B. Brown, and S. Nesic. *Effect of pH on CO2 Corrosion of Mild Steel at Elevated Temperatures.* in *Corrosion/2013 NACE International Conference & Expo. Ohio University*. 2013.
[32] Dugstad, A., H. Hemmer, and M. Seiersten. *Effect of steel microstructure upon corrosion rate and protective iron carbonate film formation*. in *CORROSION 2000*. 2000. NACE International.
[33] Seikh, A.H., *Influence of Heat Treatment on the Corrosion of Microalloyed Steel in Sodium Chloride Solution.* Journal of Chemistry, 2013. 2013.
[34] G102-89, A., *Standard practice for calculation of corrosion rates and related information from electrochemical measurements*. 1999, ASTM International West Conshohocken, Pa.
[35] Tait, W.S., *An introduction to electrochemical corrosion testing for practicing engineers and scientists*. 1994: Clair, Racine, Wis.